Chemical Engineering Science 77 (2012) 2–9

Contents lists available at SciVerse ScienceDirect

Chemical Engineering Science

journal homepage: www.elsevier.com/locate/ces

Towards achieving a flattop crystal size distribution by continuous seeding and controlled growth

Mo Jiang [a,b], Min Hao Wong [a], Zhilong Zhu [a,b], Jieqian Zhang [a], Lifang Zhou [a,b], Ke Wang [a], Ashlee N. Ford Versypt [a], Tong Si [a], Lisa M. Hasenberg [a,b], Yao-En Li [c], Richard D. Braatz [a,b,*]

[a] University of Illinois at Urbana-Champaign, Urbana, IL 61801, USA
[b] Massachusetts Institute of Technology, 77 Massachusetts Avenue, Room 66-372, Cambridge, MA 02139, USA
[c] Abbott Laboratories, Abbott Park, IL 60064, USA

ARTICLE INFO

Article history:
Received 7 September 2011
Received in revised form
28 November 2011
Accepted 20 December 2011
Available online 20 January 2012

Keywords:
Concentration feedback control
Crystallizer design
Dual impinging jets
Process intensification
Crystallization
Pharmaceuticals

ABSTRACT

A semi-continuous crystallizer configuration that combines continuous seeding using a dual impinging jet with growth rate control in a stirred tank was experimentally demonstrated for the manufacture of L-asparagine monohydrate (LAM) crystals with the objective of obtaining a target flattop size distribution. The dual impinging jets combined hot and cold saturated solutions to generate highly uniform 20-μm crystals that were further grown to a desired size in the stirred tank with suppressed nucleation that was instrumented with attenuated total reflection–Fourier transform infrared (ATR–FTIR) spectroscopy and focused beam reflectance measurement (FBRM). The construction of calibration models and the measurement of solubility and metastable limit were obtained by an automated system that followed preset supersaturation profiles using feedback control. The experiments confirm that greatly enhanced control of the crystal size distribution can be achieved using continuous seeding.

© 2012 Elsevier Ltd. All rights reserved.

1. Introduction

A control objective in the pharmaceutical industry is to manufacture crystals with a desired size distribution, so as to meet bioavailability requirements such as for inhalers or pulmonary delivery (Nagao et al., 2005; Rasenack et al., 2003; Shekunov and York, 2000). As described in these papers and elsewhere, the desired crystal size distribution for many pharmaceutical delivery applications is not necessarily the narrowest, and can have tight specifications within certain size ranges. Improved distribution control can also eliminate or reduce the amount of post-crystallization processing such as milling that can cause changes in polymorphic identity (Alleso et al., 2010; Am Ende and Brenek, 2004; Descamps et al., 2007; Lin et al., 2010; Linol et al., 2007; Tian et al., 2010) and can enable the manufacture of size distributions with higher surface area during operations to reduce the likelihood of uncontrolled nucleation being induced by changes in contaminant profiles. Various methods have been proposed to control the size distribution during organic or inorganic crystallizations (Aamir et al., 2010; Grön et al., 2003; Larsen et al., 2006; Lee et al., 2002; Liotta and Sabesan, 2004; Nagy et al., 2008; Rohani et al., 2005; Wibowo et al., 2001; Worlitscheck and Mazzotti, 2004).

The controllability of the crystal size distribution is limited in industrial batch crystallizations, in which seed crystals are added near the start of the batch, especially when multiple concurrent phenomena can occur such as growth, aggregation, and nucleation, which can also have multiple concurrent mechanisms (Ward et al., 2006). A theoretical study predicted that the controllability of the crystal size distribution could be greatly increased by employing *continuous seeding*, where crystals are continuously fed to a well-mixed tank crystallizer at any times during the batch (Woo et al., 2007, 2011). The stirred tank was assumed to operate at a controlled size-independent growth rate by applying concentration feedback control (Fujiwara et al., 2002; Nagy et al., 2008), which has produced negligible nucleation in numerous pharmaceutical crystallizations in academic and industrial laboratories (Fujiwara et al., 2002; Kee et al., 2009a, 2011; Nagy et al., 2008; Grön et al., 2003; Zhou et al., 2006). Aggregation was assumed to be suppressed by judicious selection of seed crystals, in particular, feeding the seed crystals in a slurry and selecting crystals large enough to avoid sticking together. In the concentration feedback control strategy, the control system adjusted the temperature or addition rate to track a setpoint trajectory in the crystallization phase diagram (Nagy et al., 2008). The insensitivity of this approach to most variations in growth and nucleation kinetics and most practical disturbances has been demonstrated in experiments and simulations for many batch

* Corresponding author at: Massachusetts Institute of Technology, 77 Massachusetts Avenue, Room 66-372, Cambridge, MA 02139, USA. Fax: +1 617 258 0546.
E-mail address: braatz@mit.edu (R.D. Braatz).

0009-2509/$ - see front matter © 2012 Elsevier Ltd. All rights reserved.
doi:10.1016/j.ces.2011.12.033

cooling and antisolvent crystallizations in polymorphic and non-polymorphic systems (Jiang et al., 2011; Nagy et al., 2008).

The main objective of this paper is to experimentally demonstrate the ability of continuous seeding to produce a nearly flattop crystal size distribution, which is a shape that has never been reported as the product of a batch cooling crystallization. In this approach, the crystal nucleation and growth processes are decoupled. Seed crystals are continuously added at appropriate times to a well-mixed cooling crystallizer operating under conditions of growth with negligible nucleation. There are many ways to generate these seed crystals (in a slurry) continuously. One common approach is to combine solution and antisolvent streams in dual impinging jets (DIJs), which can produce crystals of narrow size distribution for many solute–solvents systems (Johnson and Prud'homme, 2003; Mahajan and Kirwan, 1994; Midler et al., 1994). At appropriate flow rates, the dual impinging jets can generate high-intensity micromixing of fluids to quickly achieve a nearly homogeneous composition of high supersaturation before the onset of primary homogeneous nucleation so that the exit crystals have a narrow and reproducible size distribution. In contrast to the literature, this paper utilizes a DIJ configuration that combines hot and cold saturated solutions to generate seed crystals with a narrow size distribution, to exploit the fact that the micromixing is not truly instantaneous, so that supersaturations high enough for primary homogeneous nucleation are generated before complete mixing occurs. To our knowledge, this is the first time that experimental data have been reported for such a cooling DIJ.

2. Experimental methods

This section summarizes the experimental methods for characterization of the solubility, metastable limit, and growth kinetics for L-asparagine monohydrate (LAM) in aqueous solution by attenuated total reflection–Fourier transform infrared (ATR–FTIR) spectroscopy, chemometrics, and focused beam reflectance measurement (FBRM). Also discussed are the operations of the cooling DIJ and mixing-tank crystallizers that are coupled for the purpose of generating a target crystal size distribution.

2.1. Materials and instrumentation

Infrared spectra for L-asparagine monohydrate (LAM, from Sigma Aldrich) in de-ionized (DI) water were collected in a 2-l stirred tank by an in situ Dipper-210 ATR immersion probe (Axiom Analytical) with ZnSe as the internal reflectance element attached to a Nicolet 6700 FTIR spectrophotometer, 64 scans collected for each spectrum, and DI water at 25 °C used for the background (see Fig. 1). This solute–solvent system was selected because its solubility vs. temperature relationship is very similar to many pharmaceutical compounds.

During crystallization, the temperature of the slurry in the stirred tank was controlled by circulating hot and cold water to the jacket of a round-bottom or cylindrical flask with a control valve using a proportional-integral control system designed via internal model control (Kee et al., 2009a) and was measured every 2 s using a Teflon-coated thermocouple attached to a Data Translation 3004 data acquisition board via a Fluke 80 TK thermocouple module (Kee et al., 2009b). The total counts/second of LAM crystals in solution were measured every 10 s using Lasentec FBRM with version 6.0b12 of the FBRM control interface software (Kee et al., 2009a). Images of crystal slurries were taken with a polarized microscope (Leica DMI 4000B) with cameras QImaging ReRIGA 2000R (black and white) and Leica DFC 420 (color). Both FBRM and microscope can measure characteristic sizes in the range of about 1–2000 μm. Experimental data were archived and DIJ inlet flows specified using PI software from OSIsoft.

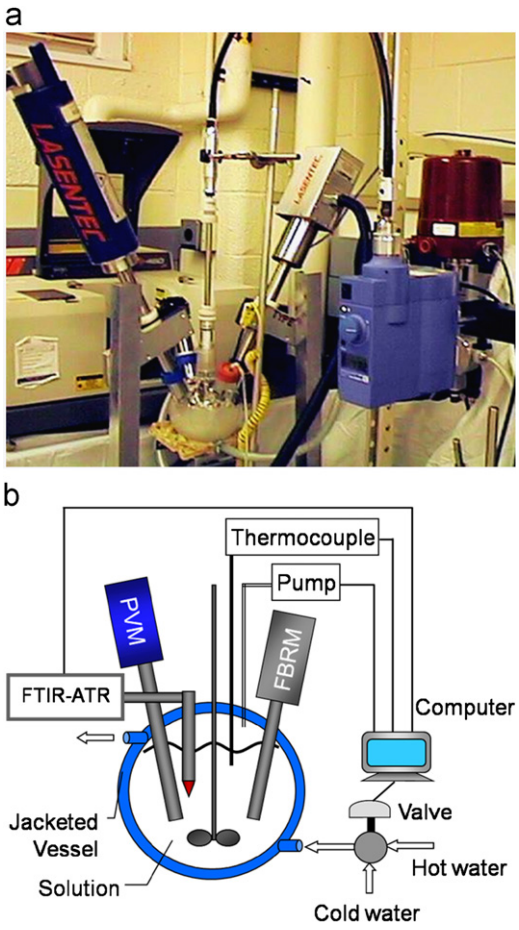

Fig. 1. Photograph (a) and schematic (b) of stirred-tank crystallizer instrumented with in situ ATR–FTIR immersion probe, FBRM probe and thermocouple. The PVM and pump was not used in this study.

Table 1
ATR–FTIR calibration samples for in situ solute concentration measurement.

Calibration sample	Solute concentration (g/g solvent)	Temperature range (°C)	Number of spectra
Cs1	0.0300	30.4–18.0	27
Cs2	0.0567	42.9–25.1	38
Cs3	0.0834	50.9–34.5	35
Cs4	0.1101	59.4–46.9	27
Cs5	0.1368	63.9–57.1	16

2.2. Calibration of ATR–FTIR for solute concentration

A bench-scale stirred-tank crystallizer was cooled at a constant rate of 0.5 °C/min for different known LAM concentrations (Table 1) in about 400 g of aqueous solution, while being measured with in situ ATR–FTIR spectroscopy and FBRM, until an increase in the total counts/s indicated that the metastable limit was reached (the detailed experimental procedures are described elsewhere (Fujiwara et al., 2002)). The width of the metastable zone at this cooling rate depended on solute concentration, so that a different number of infrared spectra was collected for each temperature.

Several chemometrics methods were applied to the absorbance spectra (in the range 1200–1800 cm^{-1}) with known solute concentrations and temperatures to construct a linear calibration model for measurement of the solute concentration (see Fig. 2) for representative data and the regression coefficients, with the

equipment and procedures being the same as for other solute–solvent systems (Fujiwara et al., 2002; Togkalidou et al., 2001). The calculations were carried out using in-house MATLAB 5.3 (The Mathworks, Inc.) code except for partial least-squares (PLS) regression, which was from the PLS Toolbox 2.0 (Eigenvector Research, Inc.). The correlation Forward Selection 2 PCR method with a noise level of 0.004 gave the smallest prediction interval of ± 0.00579 g/g solvent while being consistent with the accuracy of the solubility data. The calibration model had the form

$$C = \sum_{j=1200}^{1800} w_j a_j + w_T T + w_0 \quad (1)$$

where C is the solute concentration (g LAM/g water), a_j is the absorbance at frequency j (cm^{-1}), T is the temperature (°C), and w_j, w_T, and w_0 are regression coefficients.

2.3. Solubility measurement

The IR spectra were collected at different temperatures in an automated experimental system. At each elevated temperature, the slurry was equilibrated for at least one hour before IR spectra were recorded. The equilibration time was enough for the total counts/s to approach a constant value within the measurement noise. The solubility measurements were performed at five values of increasing temperature. The solvent mass and solute concentrations in the solubility experiments were very close to those used in the calibration experiments. The solute concentration was then calculated with the calibration model (Fig. 2b) to measure solubilities (see Fig. 3a).

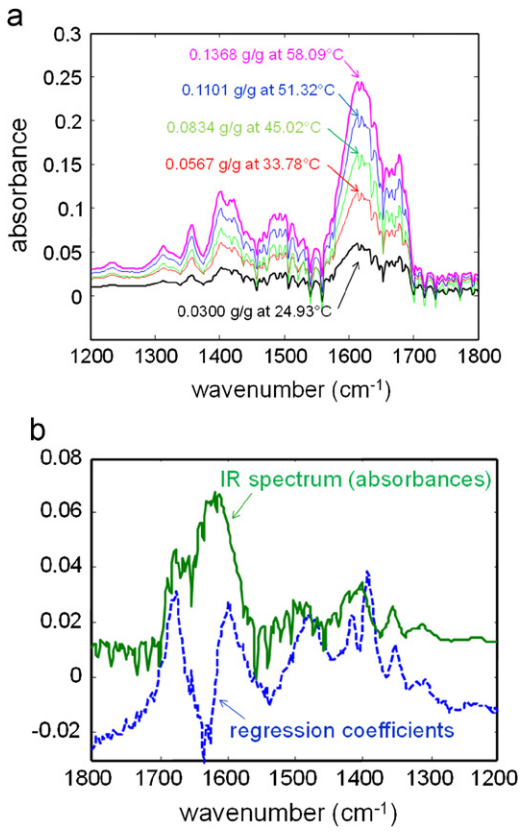

Fig. 2. (a) Representative ATR–FTIR spectra of LAM aqueous samples used for calibration (units: g LAM/g water). (b) Regression coefficients of the calibration model relating absorbances to solute concentration. The calibration model was constructed with chemometrics software (Togkalidou et al., 2001), with error less than 0.5 mg LAM/g solvent.

2.4. Seeded batch crystallizations

An initial set of seeded batch crystallizations were carried out to (*i*) verify that concentration feedback control could reliably track a constant absolute supersaturation with negligible nucleation and (*ii*) estimate average growth kinetics. An undersaturated solution with solute concentration 0.122 g LAM/g water was cooled at 0.5 °C/min from 65 °C to below the saturation temperature (55.5 °C, see Fig. 3b). The stirring conditions were very similar to the calibration experiments. Then seed crystals of LAM with mass 6.44% of the expected crystal yield were added to the solution. The seed crystals (Fig. 4a) were generated from crash cooling of high temperature LAM-saturated solution, followed by filtration and vacuum drying at room temperature and then sieving. Crash cooling usually produces a wide size distribution of crystals; to make full use of material, dry seeds of adjacent sieve ranges were combined for the concentration control experiments.

During continuous seeding, the product CSD is a function of the supersaturation (Woo et al., 2011). For each batch cooling crystallization, the control algorithm to follow a preset supersaturation profile started shortly after seeding, and continued throughout the rest of crystallization experiment (until the system cooled to about 18 °C) (Kee et al., 2009a). The supersaturation set point profiles were selected within the metastable zone at different constant absolute supersaturations ($\Delta C = C - C_{sat}$) where C_{sat} denotes the solubility

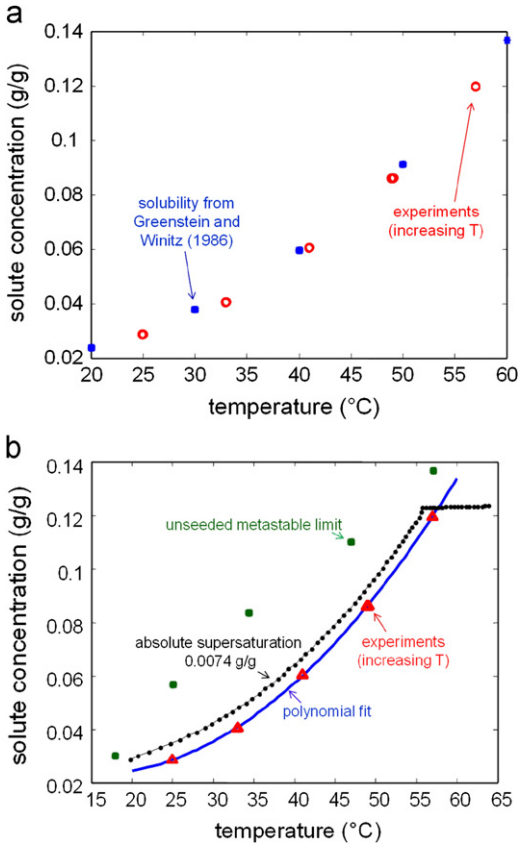

Fig. 3. (a) LAM solubility curve compared to reference data from Greenstein and Winitz (1986). Reference data are slightly higher than solute concentrations determined from the calibration model, probably due to the use of different grades of water. (b) Representative experimental solute concentrations and temperatures obtained during concentration feedback control for a constant supersaturation level of 0.0074 g/g and a seeding point at 55.5 °C. Also shown is the unseeded metastable limit that defines the highest solute concentration for which the calibration model was valid, which is much higher than the solute concentrations used in the concentration feedback control experiments.

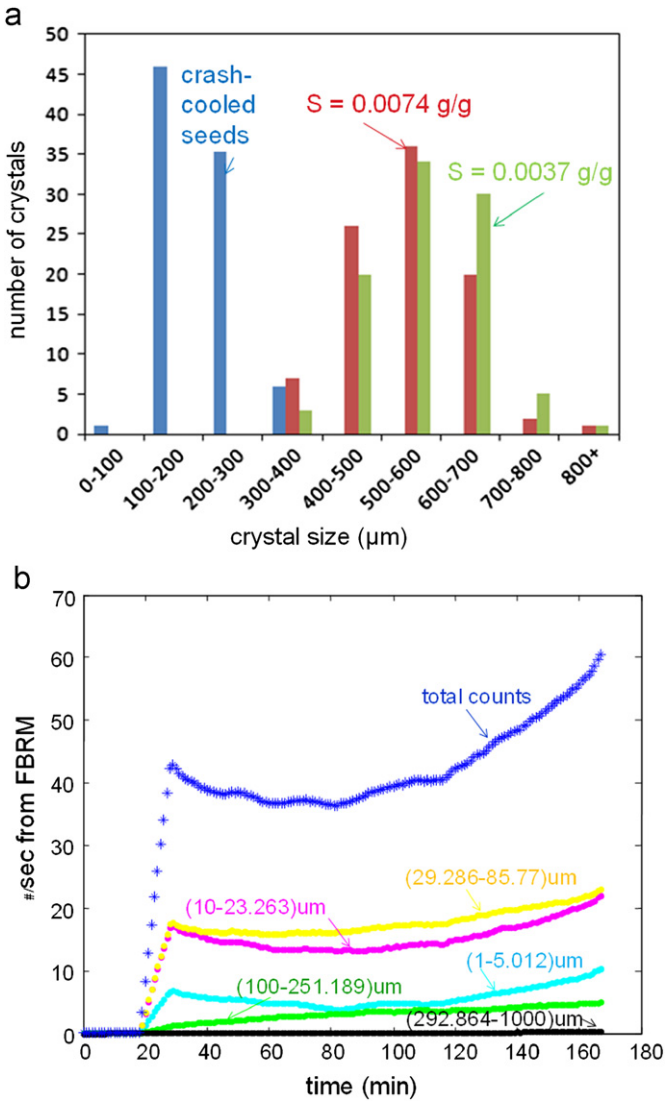

Fig. 4. (a) Size distribution of LAM seeds (based on the largest dimension) and product crystals after concentration feedback control at two different values of constant supersaturation, measured from off-line optical microscopy. (b) FBRM counts during concentration feedback control at constant supersaturation of 0.0074 g LAM/g water.

(g LAM/g water). In addition to visual inspection by optical microscopy after each experiment, FBRM data collected during each experiment confirmed that negligible nucleation occurred (see Fig. 4b).

These experiments with seeds obtained by crash cooling serve to demonstrate good concentration feedback control for the system and, at same time, estimation of temperature-averaged growth rates.[1] As dry seed crystals have a tendency to agglomerate, slurry seed crystals were used in subsequent experiments. More specifically, for implementation towards the production of a target crystal size distribution, slurry seeds manufactured by dual impinging jets (Fig. 5, details below) with size less than 20 μm (Fig. 6) were fed to the stirred tank through the crystallizer neck (with residence time of about 1 s). The total mass of seeds added in slurry form was 3.39% of the total expected crystal yield. Similarly, the feedback control algorithm started shortly after seeding, and continued throughout the cooling crystallization experiment.

[1] For example, as used by Farrell and Tsai (1994); Matthews and Rawlings (1998); Qiu and Rasmuson (1994).

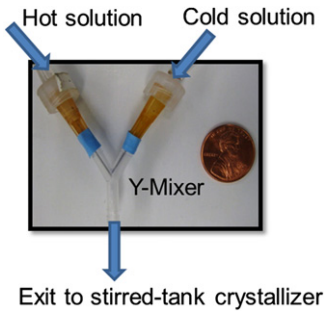

Fig. 5. Photograph of DIJ configuration for continuous seeding coupled to a stirred-tank crystallizer. Needles were inserted into a standard plastic Y-mixer to generate the seed crystals in Fig. 6.

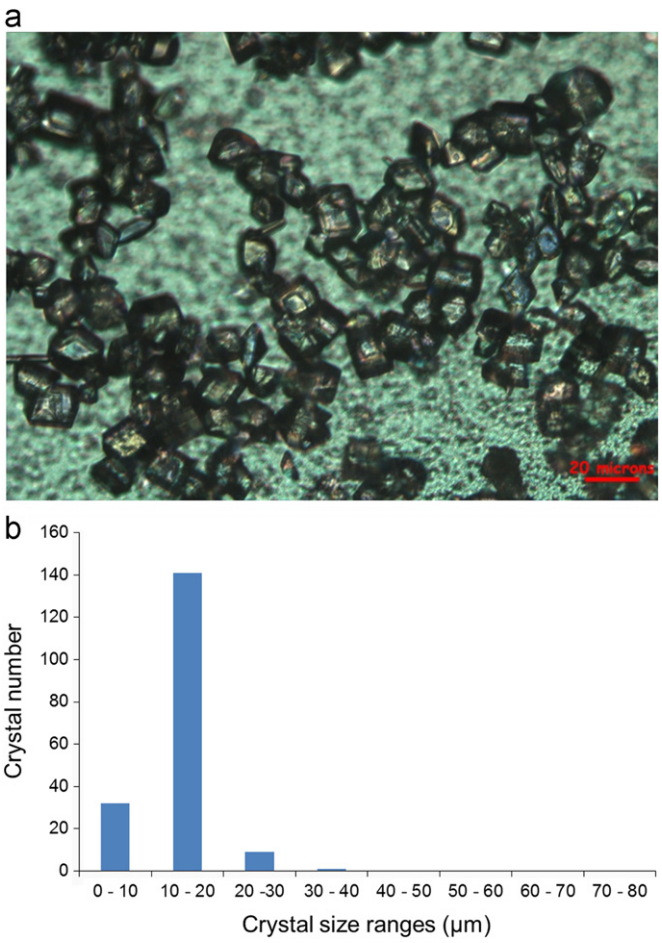

Fig. 6. LAM crystals generated by DIJs (scale bar=20 μm) (a) Microscopy image (with polarizers) and (b) Size distribution measured from off-line microscopy images.

2.5. Continuous seeding using dual impinging jets

The crystallizer configuration for the manufacture towards a target size distribution used in this particular experimental implementation (Fig. 5) employed a dual-impinging-jet (DIJ) mixer (Johnson and Prud'homme, 2003; Mahajan and Kirwan, 1994; Midler et al., 1994) in the shape of a Y to produce seed crystals that were continuously dropped into a 2-l stirred-tank cooling crystallizer operating under concentration feedback control following a preset constant supersaturation (0.01 g LAM/g water) profile, to exactly

correspond to the continuous seeding crystallizer configuration investigated in an earlier theoretical study by Woo et al. (2007, 2011). The stirred-tank crystallizer initially contained 1363 ml of saturated solution. The theoretical study indicated that the extra degrees of freedom provided by continuous seeding, instead of only seeding at the start of the crystallization, greatly increase the controllability of the crystal size distribution. A flattop size distribution was selected for experimental validation of the approach as its shape is very different from the product size distributions produced by cooling crystallizations that only seed at the beginning of the batch. As the optimal jet velocity profile for producing the flattop CSD was nearly constant, to simplify the implementation the experiments employed a constant jet velocity of 1.9 m/s, with a volumetric flow rate of 5.8 ml/min and jet inner diameter of 0.254 mm. The total slurry volume added during the experiment was 88.5 ml. For crystallization with neither nucleation nor aggregation, multiplying the supersaturation and/or mass flow rate of seeds by a constant changes the height and width of the flattop distribution with negligible effect on its shape (for detailed mathematical expressions, see Woo et al. (2007, 2011)), so the theoretically optimal distribution shape can be directly compared to the experimentally obtained distribution for a different solute–solvent system (see Fig. 10, measured manually from off-line microscope images of hundreds of crystals). Due to the limited volume limit of the stirred-tank crystallizer, for proof-of-concept purposes, the continuous seeding was allowed to cover a 4.4% volume ratio of the reactor. The seeding time duration could also help tune the width of the product CSD.

Unlike antisolvent/reaction DIJ crystallizations, this experimental implementation generated seed crystals by mixing hot and cold saturated streams (solution concentrations of 0.20 g LAM/g water at 70 °C and 0.03 g LAM/g water at 25 °C). If the micromixing were perfect, then it is straightforward to show from a mass balance and Fig. 3a that the solute concentration of the well-mixed stream for this solute–solvent system would be near saturated conditions, with supersaturation too low ($(C-C_{sat})/C_{sat}=1.4$) to generate nuclei by primary homogeneous nucleation. Crystals nucleate easily from this cooling DIJ configuration, suggesting that the micromixing is sufficiently slow in this system that high enough supersaturation is generated near the interfaces between the two streams to induce nucleation.

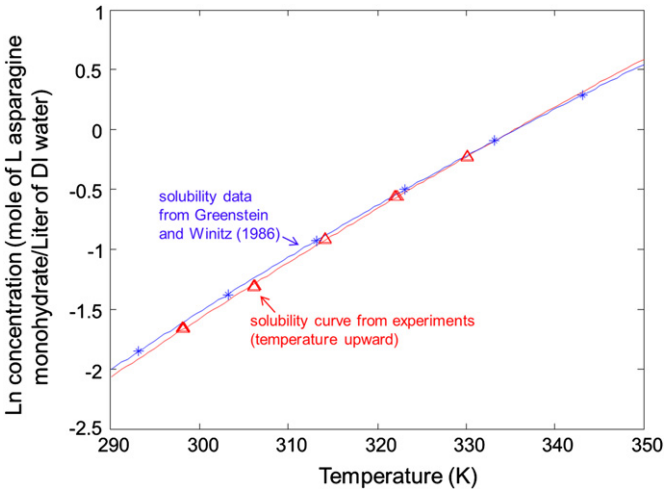

Fig. 7. Van't Hoff equation, $\ln C_0 = 9973.791T^{-1} + 86.14549\ln T - 56.68014$, fit to solubilities for LAM in aqueous solution obtained from ATR–FTIR spectroscopy (red triangles). A van't Hoff equation was also fit to previously published solubility data from Greenstein and Winitz (1986) that are shown as blue asterisks. (For interpretation of the references to colour in this figure legend, the reader is referred to the web version of this article.)

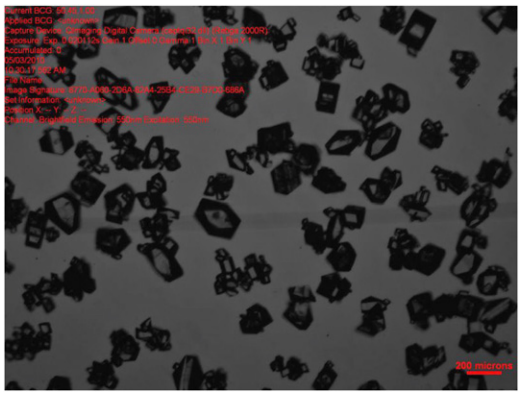

Fig. 8. Microscope image of a batch of LAM seed crystals after sieving for the range 125–180 μm (scale bar=200 μm).

3. Results and discussion

3.1. Solubility

The solubility curve of LAM in aqueous solution was fit to a quadratic function to give

$$C_{sat} = 3.084 \times 10^{-2} - 1.373 \times 10^{-3} T + 5.214 \times 10^{-5} T^2 \quad (2)$$

(see Fig. 3b). The maximum deviation of the experimental data points from the fitted solubility curves (0.0021 g LAM/g water) was within the prediction intervals. The solubility data were also fit to a van't Hoff equation (Grant et al., 1984):

$$\ln C_0 = -(a/R)T^{-1} + (b/R)\ln T + c \quad (3)$$

where R is the ideal gas constant, T is in units of Kelvin, and C_0 is in units of mole fraction (see Fig. 7). The solubility data are in good agreement with Greenstein and Winitz (1986); the differences can be attributed to differences in the purity of water in the two sets of experiments. From the coefficients of the solubility curve, the apparent enthalpy of solution (Grant et al., 1984), $\Delta H^* = a + bT$ of LAM in aqueous solution was calculated to be 35.66 kJ/mol at 298.15 K, and apparent heat capacity as $C_p^* = b = 86$ J/(mol-K). This calculated enthalpy of solution is in good agreement with calculation by applying the same method to the reference data by Greenstein and Winitz (1986) (35.45 kJ/mol) and directly from measurement (33.89 kJ/mol).

3.2. Initial seeded batch crystallizations

Batch crystallizations seeded with dry crystals generated by crash cooling (Fig. 8) to follow preset constant absolute supersaturation profiles within the metastable zone were implemented using concentration feedback control with cooling rate based on the in situ measurement of the solute concentration (Fig. 3b). The solute concentration very closely tracked the setpoint trajectory in the phase diagram as has been observed for many other pharmaceutical compounds (e.g., Fujiwara et al., 2002; Kee et al., 2009a).

Two sets of supersaturation profiles were applied. Run 1 was implemented at a constant supersaturation ($\Delta C = 0.0074$ g LAM/g water) that was very close to the middle of the metastable zone and Run 2 was implemented for half of this absolute supersaturation ($\Delta C = 0.0037$ g LAM/g water). Microscope images of the product crystals are very similar between the two runs (see Fig. 9a and b). Inspection of the microscope images and FBRM data (Fig. 4) indicated that negligible nucleation occurred in the stirred-tank.

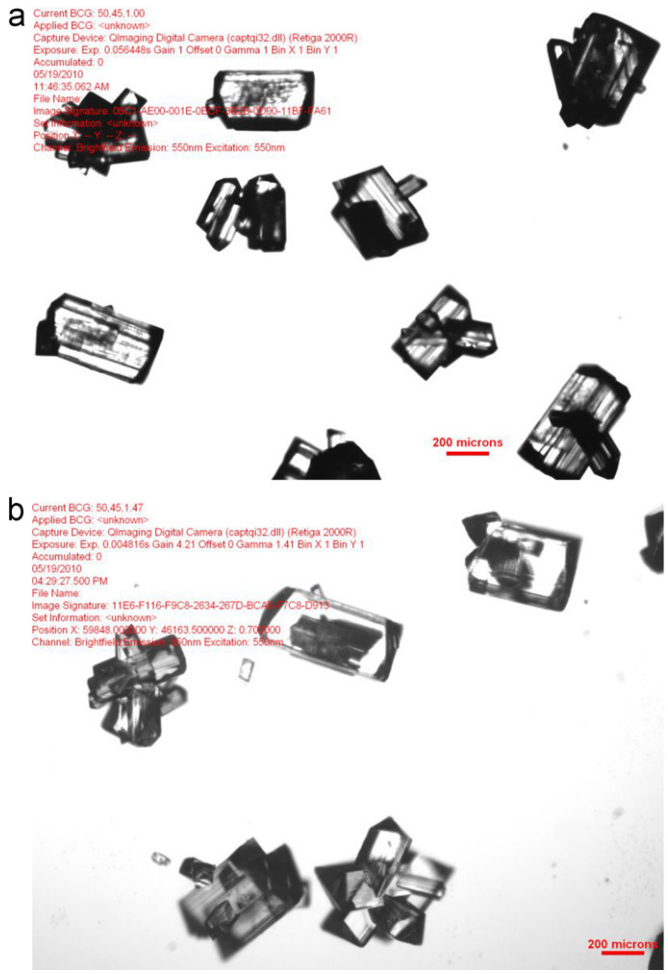

Fig. 9. Microscope images of LAM product crystals produced by concentration feedback control experiments with constant supersaturation of (a) 0.0074 g LAM/g water and (b) 0.0037 g LAM/g water (scale bar=200 μm).

The change in the mean crystal length during each experiment operating under constant absolute supersaturation in Fig. 4a was divided by the batch time to determine the average growth rate for each supersaturation. The estimated average growth rate G was plotted vs. supersaturation S to estimate the kinetic parameters in the power-law growth rate expression $G=k_gS^g$ for LAM crystals in aqueous solution, closely following a procedure described by Kee et al. (2011), which determined that $g\approx 1$ and average $k_g=6.353$ μm/s. The relationship between the average growth rate and absolute supersaturation implies that the concentration feedback control provides control of the average growth rate in the stirred-tank crystallizer.

The crystals shown in Fig. 8 were produced by crash cooling followed by vacuum drying and sieving, which caused some aggregation. Slurry seeds were used in the subsequent continuous seeding experiment because (*i*) they have a reduced potential for aggregation, and (*ii*) using a carrier fluid makes it easier to reliably deliver seed crystals at a smoothly controlled rate to a stirred-tank crystallizer.

3.3. Continuous seeding by dual impinging jets

Seed crystals produced by the DIJ mixer were highly uniform and smaller than 20 μm (Fig. 6). It is unlikely that the nucleation of these seed crystals occur under conditions of perfect mixing (that is, conditions in which the two liquids are mixed at the molecular scale before nucleation occurs). The temperature achieved by complete mixing would be about 47.5 °C, which is the average of the two inlet stream temperatures of 25 °C and 70 °C in a 1:1 volume ratio, and the solubility at that temperature is about 0.082 g LAM/g water (see Fig. 3a). If the solute concentrations were perfectly mixed, the well-mixed concentration would be (0.2+0.03)/2=0.115 g LAM/g water, which is just above the unseeded metastable limit in Fig. 3b measured for a large-volume stirred-tank crystallizer at a low cooling rate. Smaller volumes and higher cooling rates produce much higher metastable limits than for large volumes at low cooling rates (the former effect is described in papers on nucleation in microscale droplets, e.g., Goh et al., 2010, and the latter effect is described in any textbook or paper that discusses metastable limits in some detail, e.g., Fujiwara et al., 2002), which implies that the seed crystals were not nucleated under conditions of perfect mixing (which is defined in this context as the crystals nucleating after the fluids have perfectly mixed).

The ratio of the Prandtl to the Schmidt number, D/α, specifies the relative thickness of the concentration boundary layer to the thermal boundary layer, which is about 1/100, where D is the diffusivity of LAM in solution and α is the thermal diffusivity of the solution. This value indicates that the thermal boundary layer is much thicker than the concentration boundary layer. This implies that the temperature in the high concentration fluid side of the interface can drop while the concentration remains high, to produce a highly supersaturated solution. If symmetry about the interface between the two fluids is assumed, then the temperature near the interface is about equal to 47.5 °C, and a solute concentration of 0.2 g LAM/g water is far enough above the metastable limit measured in Fig. 3b to indicate that primary homogenous nucleation can occur within the 1 s of residence time before the mixture enters the mixed-tank crystallizer. Collectively, this analysis provides evidence that the two liquids were not mixed at the molecular scale before crystal nucleation occurred.

The seeds in slurry generated by the DIJ mixer were continuously added to the experimentally validated concentration-controlled stirred-tank crystallizer (Fig. 1) for manufacturing the product crystal size distribution. For this experimental validation, the use of a flattop size distribution as the target enabled a direct comparison to the previously published theoretical results by Woo et al. (2007, 2011) (see Fig. 10 for the optimal CSD for some realistic seed crystals). Most of the product crystals are within the size range of 50–150 μm, with similar smoothing at high and low sizes as

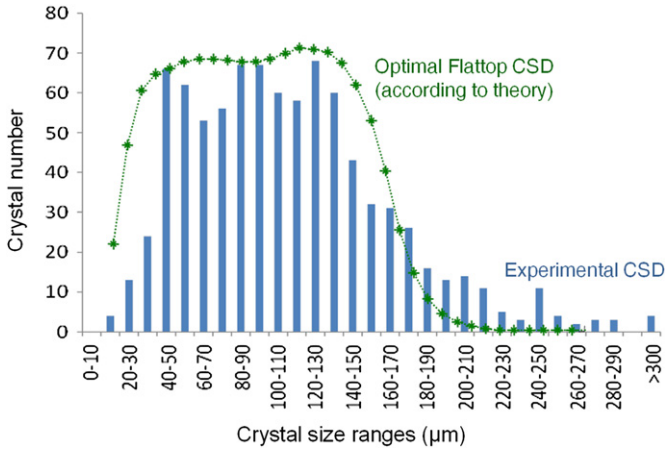

Fig. 10. Comparison of optimal flattop CSD (green plot, from Woo et al., 2011) and experimental CSD measured by off-line optical microscopy (blue histogram). (For interpretation of the references to colour in this figure legend, the reader is referred to the web version of this article.)

Fig. 11. Microscopy image (with polarizers) of LAM product crystals at the end of concentration control after continuous DIJ seeding (scale bar=100 μm).

predicted by theory for a seed distribution with nonzero width (Fig. 10). The experimental product crystal size distribution has very similar deviations from the target size distribution as predicted by theory. The theory of Woo et al. (2011) assumed no growth rate dispersion and that the crystallizer was perfectly well-mixed, and the experimentally observed longer tail at large crystal sizes in Fig. 10 could be due to growth rate dispersion or some non-ideal mixing in the crystallizers. A microscope image in Fig. 11 shows crystals with a highly uniform shape with minimum aggregation and no fine crystals as would be produced by nucleation. These results provide an experimental validation of the increased controllability of the size distribution obtainable by continuous seeding.

4. Conclusions

A semi-continuous crystallizer configuration that combines continuous seeding using dual impinging jets (DIJ) with concentration control in a stirred tank was experimentally demonstrated for the manufacture of L-asparagine monohydrate (LAM) crystals with the objective of manufacturing crystals with a flattop size distribution. The DIJ combined hot and cold saturated solutions to produce highly uniform LAM crystals with an average size less than 20 μm that were grown using the concentration controlled stirred tank operated to have minimum nucleation. The approach included the automated collection of data for the determination of the solubility curve, metastable limit, and temperature-averaged growth kinetics for LAM crystals in aqueous solution. The size distribution of the product crystals were very similar to that predicted as being achievable in a published theoretical study.

In this approach, the DIJ crystallizer can be replaced by any alternative technique for the continuous generation of seeds, as long as the rate of production of seed crystals can be specified and the seed crystals are uniform and smaller than the desired length resolution in the target product size distribution. Examples of alternative continuous seeding equipment include vortex mixers and wet milling crystals from a previous batch. Dual-impinging-jet and vortex mixers generate crystals of high uniformity of size and shape and produce a higher overall crystal yield per batch than wet milling crystals from a previous batch. By keeping a low supersaturation for the entire time history of each crystal, using wet milling crystals from a previous batch as seeds may generate product crystals of higher average molecular purity.

Acknowledgments

The authors thank Abbott laboratories, Inc. for financial support, OSIsoft and Timothy O. Drews for financial and technical support for the PI system, and Mitsuko Fujiwara for technical advice on experimental implementation and input on the manuscript.

References

Aamir, E., Nagy, Z.K., Rielly, C.D., 2010. Optimal seed recipe design for crystal size distribution control for batch cooling crystallisation processes. Chem. Eng. Sci. 65, 3602–3614.
Alleso, M., Tian, F., Cornett, C., Rantanen, J., 2010. Towards effective solid form screening. J. Pharm. Sci. 99, 3711–3718.
Am Ende, D.J., Brenek, S.J., 2004. Strategies to control particle size during crystallization processes. Am. Pharm. Rev. 7 (3), 98–104.
Descamps, M., Willart, J.F., Dudognon, E., Caron, V., 2007. Transformation of pharmaceutical compounds upon milling and comilling: The role of T_g. J. Pharm. Sci. 96, 1398–1407.
Farrell, R.J., Tsai, Y.C., 1994. Modeling, simulation and kinetic parameter-estimation in batch crystallization processes. AIChE J. 40, 586–593.
Fujiwara, M., Chow, P.S., Ma, D.L., Braatz, R.D., 2002. Paracetamol crystallization using laser backscattering and ATR-FTIR spectroscopy: Metastability, agglomeration, and control. Cryst. Growth Des. 2, 363–370.
Goh, L., Chen, K.J., Bhamidi, V., He, G.W., Kee, N.C.S., Kenis, P.J.A., Zukoski III, C.F., Braatz, R.D., 2010. A stochastic model for nucleation kinetics determination in droplet-based microfluidic systems. Cryst. Growth Des. 10, 2515–2521.
Grant, D.J.W., Mehdizadeh, M., Chow, A.H.-L., Fairbrother, J.E., 1984. Non-linear van't Hoff solubility-temperature plots and their pharmaceutical interpretation. Int. J. Pharm. 18, 25–33.
Greenstein, J.P., Winitz, M., 1986. Chemistry of the Amino Acids. Robert. E. Krieger Publishing Company, Malabar, FL.
Grön, H., Borissova, A., Roberts, K.J., 2003. In-process ATR-FTIR spectroscopy for closed-loop supersaturation control of a batch crystallizer producing monosodium glutamate crystals of defined size. Ind. Eng. Chem. Res. 42, 198–206.
Jiang, M., Woo, X.Y., Kee, N.C.S., Goh, L.M., Tice, J.D., Zhou, L., Tan, R.B.H., Zukoski III, C.F., Fujiwara, M., Nagy, Z.K., Kenis, P.J.A., Braatz, R.D., 2011. The role of automatic process control in Quality by Design. In Quality by Design. John Wiley & Sons, New York. in press.
Johnson, B.K., Prud'homme, R., 2003. Chemical processing and micromixing in confined impinging jets. AIChE J. 49, 2264–2282.
Kee, N.C.S., Tan, R.B.H., Braatz, R.D., 2009a. Selective crystallization of the metastable alpha-form of L-glutamic acid using concentration feedback control. Cryst. Growth Des. 9, 3044–3051.
Kee, N.C.S., Arendt, P.D., Tan, R.B.H., Braatz, R.D., 2009b. Selective crystallization of the metastable anhydrate form in the enantiotropic pseudo-dimorph system of L-phenylalanine using concentration feedback control. Cryst. Growth Des. 9, 3052–3061.
Kee, N.C.S., Arendt, P.D., Goh, L.M., Tan, R.B.H., Braatz, R.D., 2011. Nucleation and growth kinetics estimation for L-phenylalanine hydrate and anhydrate crystallization. Cryst. Eng. Comm. 13, 1197–1209.
Larsen, P.A., Patience, D.B., Rawlings, J.B., 2006. Industrial crystallization process control. IEEE Control Syst. Mag. 26, 70–80.
Lee, K., Lee, J.H., Fujiwara, M., Ma, D.L., Braatz, R.D., 2002. Run-to-run control of multidimensional crystal size distribution in a batch crystallizer. Proc. Am. Control Conference, 1013–1018.
Lin, S.-Y., Hsu, C.-H., Ke, W.-T., 2010. Solid-state transformation of different gabapentin polymorphs upon milling and co-milling. Int. J. Pharm. 396, 83–90.
Linol, J., Morelli, T., Petit, M.N., Coquerel, G., 2007. Inversion of the relative stability between two polymorphic forms of (±) modafinil under dry high-energy milling: Comparisons with results obtained under wet high-energy milling. Cryst. Growth Des. 7, 1608–1611.
Liotta, V., Sabesan, V., 2004. Monitoring and feedback control of supersaturation using ATR-FTIR to produce an active pharmaceutical ingredient of a desired crystal size. Org. Process Res. Dev. 8, 488–494.
Mahajan, A.J., Kirwan, D.J., 1994. Nucleation and growth-kinetics of biochemicals measured at high supersaturations. J. Cryst. Growth 144, 281–290.
Matthews, H.B., Rawlings, J.B., 1998. Batch crystallization of a photochemical: Modeling, control, and filtration. AIChE J. 44, 1119–1127.
Midler, Jr., M., Paul, E.L., Whittington, E.F., Futran, M., Liu, P.D., Hsu, J., Pan, S.-H., 1994. Crystallization method to improve crystal structure and size. U.S. Patent 5,314,506.
Nagao, L.M., Lyapustina, S., Munos, M.K., Capizzi, M.D., 2005. Aspects of particle science and regulation in pharmaceutical inhalation drug products. Cryst. Growth Des. 5, 2261–2267.
Nagy, Z.K., Chew, J.W., Fujiwara, M., Braatz, R.D., 2008. Comparative performance of concentration and temperature controlled batch crystallizations. J. Process Control 18, 399–407.
Qiu, Y.F., Rasmuson, Å.C., 1994. Estimation of crystallization kinetics from batch cooling experiments. AIChE J. 40, 799–812.
Rasenack, N., Steckel, H., Muller, B.W., 2003. Micronization of anti-inflammatory drugs for pulmonary delivery by a controlled crystallization process. J. Pharm. Sci. 92, 35–44.

Rohani, S., Horne, S., Murthy, K., 2005. Control of product quality in batch crystallization of pharmaceuticals and fine chemicals. Part 2: External control. Org. Process Res. Dev. 9, 873–883.
Shekunov, B.Y., York, P., 2000. Crystallization processes in pharmaceutical technology and drug delivery design. J. Cryst. Growth 211, 122–136.
Tian, F., Qu, H., Louhi-Kultanen, M., Rantanen, J., 2010. Insight into crystallization mechanisms of polymorphic hydrate systems. Chem. Eng. Technol. 33, 833–838.
Togkalidou, T., Fujiwara, M., Patel, S.D., Braatz, R.D., 2001. Solute concentration prediction using chemometrics and ATR-FTIR spectroscopy. J. Cryst. Growth 231, 534–543.
Ward, J.D., Mellichamp, D.A., Doherty, M.F., 2006. Choosing an operating policy for seeded batch crystallization. AIChE J. 52, 2046–2054.
Wibowo, C., Chang, W.C., Ng, K.M., 2001. Design of integrated crystallization systems. AIChE J. 47, 2474–2492.
Woo, X.Y., 2007. Modeling and Simulation of Antisolvent Crystallization: Mixing and Control. Ph.D. thesis, University of Illinois, Urbana-Champaign and National University of Singapore.
Woo, W.Y., Tan, R.B.H., Braatz, R.D., 2011. Precise tailoring of the crystal size distribution by controlled growth and continuous seeding from impinging jet crystallizers. Cryst. Eng. Comm. 13, 2006–2014.
Worlitschek, J., Mazzotti, M., 2004. Model-based optimization of particle size distribution in batch-cooling crystallization of paracetamol. Cryst. Growth Des. 4, 891–903.
Zhou, G.X., Fujiwara, M., Woo, X.Y., Rusli, E., Tung, H.-H., Starbuck, C., Davidson, O., Ge, Z., Braatz, R.D., 2006. Direct design of pharmaceutical antisolvent crystallization through concentration control. Cryst. Growth Des. 6, 892–898.